Available online at www.sciencedirect.com
ScienceDirect
Trans. Nonferrous Met. Soc. China 24(2014) 3639−3644
Transactions of Nonferrous Metals Society of China
www.tnmsc.cn

Comparative analysis of isothermal and non-isothermal solidification of binary alloys using phase-field model

Rong-zhen XIAO, Guo-sheng AN, Chang-sheng ZHU, Zhi-ping WANG, Shi-yin YANG

State Key Laboratory of Gansu Advanced Non-ferrous Metal Materials, Lanzhou University of Technology, Lanzhou 730050, China

Received 18 December 2013; accepted 1 April 2014

Abstract: Based on the entropy function, a two-dimensional phase field model of binary alloys was established. Meanwhile, an explicit difference method with uniform grid was adopted to solve the phase field and solute field controlled equations. And the alternating direction implicit (ADI) algorithm for solving temperature field controlled equation was also employed to avoid the restriction of time step. Some characteristics of the Ni−Cu alloy were captured in the process of non-isothermal solidification, and the comparative analysis of the isothermal and the non-isothermal solidification was investigated. The simulation results indicate that the non-isothermal model is favorable to simulate the real solidification process of binary alloys, and when the thermal diffusivity decreases, the non-isothermal phase-field model is gradually consistent with the isothermal phase-field model.

Key words: phase-field model; binary alloys; isothermal solidification; non-isothermal solidification

1 Introduction

Microstructures are formed at moving liquid−solid interface, and the equiaxed dendritic solidification is a frequently observed mode in the process of solidification. In addition to some experimental methods, a large number of numerical methods are involved in solidification and materials processing [1−4]. As one of the numerical simulation methods to elucidate the complex microstructure evolution, the phase-field method has been widely accepted by researchers [5−8]. The phase-field model (PFM) is known to be powerful in describing the complex formation in the process of solidification, because all the controlling equations are given as unified forms in the whole space of system. And the phase-field method does not have to strictly distinguish the solid and liquid, thus it avoids the difficulty of tracking the complex liquid−solid interface [9−11].

In the solidification process of binary alloys, the solidification rate is limited by both heat and solute diffusion, and the heat and solute diffusion fields are coupled at the solid−liquid interface by the relations with flux balances. The first PFM for alloy isothermal solidification based on the free energy function was proposed by WHEELER et al [9], and it was widely called WBM I mode. In this model, the term of $(\nabla\phi)^2$ is embodied in the governing equations, but the situations of solute trapping are not exhibited because of neglecting the term of $(\nabla c)^2$, then such situations are frequently observed experimentally. Thereby, WHEELER et al [12] advanced a new PFM(WBM II), which incorporated both the $(\nabla\phi)^2$ and $(\nabla c)^2$ terms. But it is intriguing that some researchers confirmed that the term of $(\nabla c)^2$ is not necessary to predict solute trapping [13,14]. Another PFM for binary alloys was proposed by KIM et al [15,16], and was named KKS model. Then the KKS model is equivalent with the WBM model, but has a different definition of the free energy density for the interfacial region. For non-isothermal solidification, the effect of temperature distribution is considered in the PFM due to release of latent heat at the liquid−solid interface. CONTI [17] discussed the thermal effects on solidification of binary alloys, and LOGINOVA et al [18] simulated the dendritic morphology and temperature distribution of Ni−Cu binary alloy using phase-field method [18]. Recently, OHNO [19] expended the PFM to ternary alloys of non-isothermal solidification, and the convergence of

Foundation item: Projects (51161011, 11364024) supported by the National Natural Science Foundation of China
Corresponding author: Rong-zhen XIAO; Tel: +86-13919307711; E-mail: xiaorongzhen@lut.cn
DOI: 10.1016/S1003-6326(14)63509-3

the simulation was investigated.

In this work, a non-isothermal phase-field model is developed for simulating the dendritic growth of Ni−Cu binary alloys. Because of the great difference between the thermal diffusivity and the solute diffusivity, the ADI algorithm is employed for solving temperature field controlled equation, and the explicit difference method with uniform grid is adopted to solve the phase field and solute field controlled equation. Some characteristics of a Ni−Cu binary alloy are captured in the process of non-isothermal solidification with phase-field method, and the comparative analysis of the simulation results for isothermal and non-isothermal solidification of binary alloys is carried out.

2 Phase-field model

The present phase-field model for non-isothermal solidification of binary alloys is derived from Ref. [17], and the terms of $(\nabla\phi)^2$ and $(\nabla c)^2$ are contained in the model. Based on the entropy function of the system, the controlling equations of the phase field, solute field and heat field can be defined as

$$\frac{\partial\phi}{\partial t}=M_\phi\{\nabla[\varepsilon^2(\theta)\nabla\phi]+\frac{\partial}{\partial y}[\varepsilon(\theta)\varepsilon'(\theta)\phi_x]-\frac{\partial}{\partial x}[\varepsilon(\theta)\varepsilon'(\theta)\phi_y]\}-[(1-c)H^{\mathrm{A}}+cH^{\mathrm{B}}] \tag{1}$$

$$\frac{\partial c}{\partial t}=\nabla D_{\mathrm{c}}[\nabla c+\frac{V_{\mathrm{m}}}{R}c(1-c)(H^{\mathrm{B}}-H^{\mathrm{A}})\nabla\phi-\frac{V_{\mathrm{m}}}{R}c(1-c)\nabla(\delta^2\nabla^2c)] \tag{2}$$

$$\frac{\partial T}{\partial t}+[(1-c)L^{\mathrm{A}}+cL^{\mathrm{B}}]\frac{p'(\phi)}{c_p}\frac{\partial\phi}{\partial t}=D_T\nabla^2T \tag{3}$$

where ϕ is the phase-field variable, and ϕ takes on 0 in solid and 1 in liquid; c is the molar fraction of a solute B in solvent A; here, A is Ni, B is Cu; T is the temperature of the system; V_{m} is the molar volume; R is the gas constant; $\varepsilon(\theta)$ represents anisotropy of the interfacial energy; M_ϕ is a phase-field parameter related to the interface dynamics, which is defined as

$$M_\phi=(1-c)M^{\mathrm{A}}+cM^{\mathrm{B}} \tag{4}$$

In Eqs. (1) and (2), H^{A} can be defined as

$$H^{\mathrm{A}}=W^{\mathrm{A}}g'(\phi)+30g(\phi)L^{\mathrm{A}}(\frac{1}{T}-\frac{1}{T_{\mathrm{m}}^{\mathrm{A}}}) \tag{5}$$

where H^{B} has the same expression as H^{A}; L^{A} is the heat latent of pure solvent A; $T_{\mathrm{m}}^{\mathrm{A}}$ is the melting point of pure solvent A.

In Eqs. (2), D_{c} is the solute diffusivity and defined as

$$D_{\mathrm{c}}=D_{\mathrm{s}}+p(\phi)(D_{\mathrm{l}}-D_{\mathrm{s}}) \tag{6}$$

where D_{s} and D_{l} are the diffusivities in the liquid and solid, respectively. In above equations, $g(\phi)$ and $p(\phi)$ are defined as

$$g(\phi)=\phi^2(1-\phi)^2 \tag{7}$$

$$p(\phi)=\phi^3(10-15\phi+6\phi^2) \tag{8}$$

In Eq. (3), c_p is the specific heat capacity. In order to simplify the calculation, $c_p^{\mathrm{A}}=c_p^{\mathrm{B}}=c_p$; D_T is the thermal diffusivity of the mixture, and solid and liquid thermal conductivities of both materials are assumed.

By solving the diffusion equations, the relationship among the phase-field parameters $M^{\mathrm{A,B}}$, $W^{\mathrm{A,B}}$, $\bar{\varepsilon}$ and the material properties can be obtained [17,20,21].

3 Numerical issues

In order to discretize the equations of the model for the second order in space and the first order in time, finite difference approximations were utilized to solve the phase field and solute field controlled equation; then, an explicit scheme was employed to advance the solution forward in time, and centered differencing approximations in space. The ADI algorithm was employed for solving temperature field controlled equation, as shown in appendix. Using the above scheme, the C Programming Code was implemented to complete the phase-field simulation based on the compatibility of VC++ platform. The Z′ero-Neumann boundary condition was imposed to the c and ϕ at the boundaries in the bulk region, and the constant boundary condition was imposed to the temperature field. They are written as

$$\frac{\partial\phi}{\partial n}=\frac{\partial c}{\partial n}=0,\quad T_\infty=T_0 \tag{9}$$

The mesh spacing Δx has to be selected low enough to ensure an accurate resolution of both the phase-field and concentration profiles in the interfacial region. For convergence, the mesh spacing Δx and the time step Δt are given by

$$\Delta t<\frac{\Delta x^2}{4D_{\mathrm{l}}} \tag{10}$$

In accordance with the convergent condition, the step spacing $\Delta y=\Delta x=2.41\times10^{-6}$ cm and the time step $\Delta t=1.1\times10^{-8}$ s. In the present work, a square computational domain of 800×800 grids was used in the simulations.

The PFM usually can be considered one of the deterministic methods, and the crystal nucleation is finished before growth. So, the initial conditions can be required as

$$(x-x_0)^2+(y-y_0)^2\le r_0^2,\ \phi=0,\ T=T_0,\ c=c_{\mathrm{s}}^{\mathrm{eq}} \tag{11}$$

$$(x-x_0)^2+(y-y_0)^2>r_0^2,\ \phi=1,\ T=T_0-\Delta T,\ c=c_\infty \tag{12}$$

where r_0 is the radius of an initial nucleus; x and y are the coordinate axes; (x_0, y_0) is the position of the initial nucleus; T_0=1574 K is the initial temperature of the solid; ΔT is the initial undercooling; c_s^{eq} is the initial concentration of solid; c_∞ is the initial concentration of liquid. Here, we take c_s^{eq}=0.3994 and c_∞=0.40831.

4 Results and discussion

For the solidification of binary alloy, the interfacial morphology is controlled by both heat and solute diffusion. The dendritic formation and temperature distribution of Ni−Cu binary alloy obtained under non-isothermal condition are shown in Fig. 1 at the growth time of 0.66 ms. Figure 1(a) shows the phase-field and concentration morphology profile. The initial temperature (T_0) is set to be 1574 K, and this disposal is consistent with the isothermal case.

It can be found that the dendritic growth shows obvious preferred orientation although the initial crystal nucleus is set to be spherical, because the anisotropy is considered in the model. The main trunks grow going with obvious necking. The side-branches grow in a direction which is perpendicular to the parent branches, and they have undergone obvious remelting during competitive growth. In the phase-field model, the growth morphology exhibits a general four-symmetry, but the details of the side arms are not perfectly symmetric. The maximum value of the solute concentration is corresponding to the region of the dendrites between the secondary arms, and the solute concentration in the primary arm's spines is relatively low, as well as in the secondary arm's spines. This is caused by the curvature effect in the process of solidification. These phenomena are consistent with the simulations of isothermal phase-field model, which can be seen in the previous work [21].

From Fig. 1(b), it can be found that dendrite growth is surrounded by thick thermal diffusion layer in the process of solidification, and the thermal gradient is apparent in the interfacial region. The temperature in the solid regions is higher than in the liquid regions, and the highest temperature is located in the region between the secondary arms. With the non-isothermal solidification, the latent heat release increases the temperature of the system, and the thermal diffusion of solid is so difficult, thus, the solid temperature increases, that is, recalescence occurs. According to the phase diagram of Ni−Cu, the enrichment of Cu will cause decline of the liquidus, and the region will be the final solidifying zone. Then, the thermal diffusion is embarrassed by the developed side-branches, which results in the highest temperature.

Figure 2 demonstrates that the highest temperature varies with time in the process of solidification. It can be seen that, the temperature of the solidifying zone rises rapidly from 1574 K to 1574.2 K, and then increases dynamically with time, but the overall deviation is in the range of 0.35 K. Because the latent heat release increases the temperature of the system, the crystal growth is restrained at higher temperatures. Then, the latent heat release per unit time is reduced at low growth velocities, and the temperature of liquid−solid interface decreases, which results in the growth velocity increasing. So, the growth velocity and thermal distribution exhibit evident

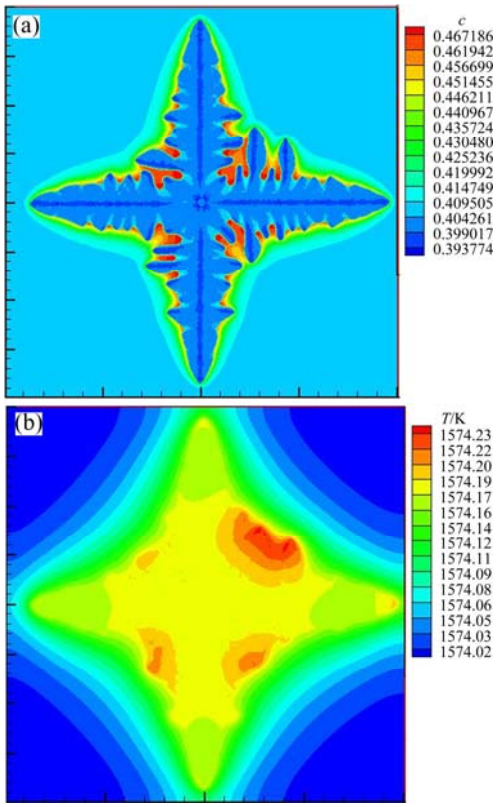

Fig. 1 Dendritic morphology and thermal distribution of non-isothermal phase-field modeling: (a) Phase field and concentration field; (b) Temperature field

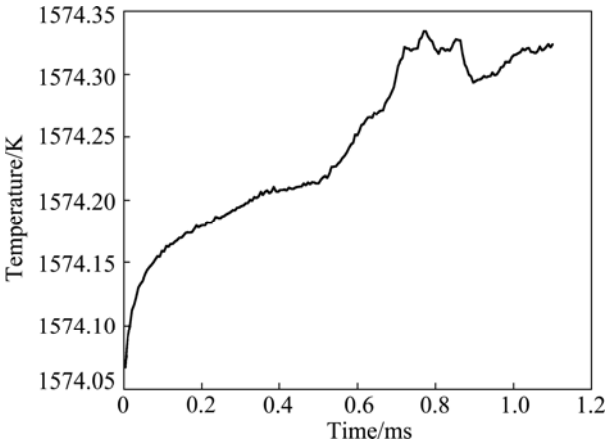

Fig. 2 Variety of the highest temperature with time

fluctuation.

Figure 3 shows the tip velocity—time curves with isothermal and non-isothermal solidification. It can be found that, the stable value of tip velocity is convergent rapidly in isothermal simulation, although a trivial fluctuation occurs. The tip velocity of non-isothermal simulation is difficult to converge to a stable value, but fluctuates acutely, and the fluctuation cycle is about 0.1 ms. Generally, the tip velocity of isothermal simulation is slightly higher than that obtained in non-isothermal simulation. The solute concentration profiles in the growth direction through a dendritic tip at different solidifying conditions are shown in Fig. 4 at the growth time of 0.8 ms. Here, the position of solute peak value corresponds to the interfacial position. It can be found that the simulation results of the two cases are consistent with the classical solidification theory, but the solid solute concentration of non-isothermal simulation is slightly higher than that obtained with isothermal model. As a whole, the solid diffusivity (~10^{-9} cm/s) is significantly lower than the growth velocity, and the solute in the solid has no enough time to be redistributed. But the solute diffuses more sufficiently with the non-isothermal solidification, because the latent heat release is taken into account, which causes a decrease in growth speed.

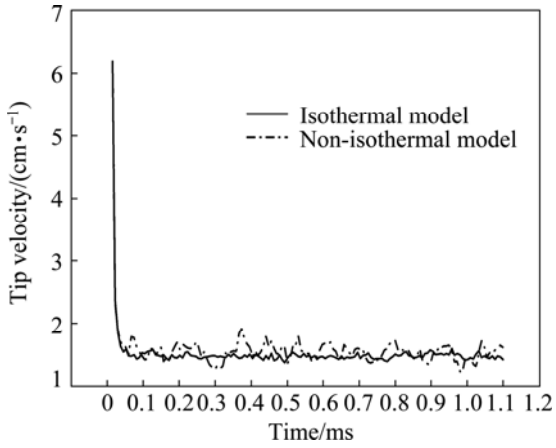

Fig. 3 Variety of tip velocity with time

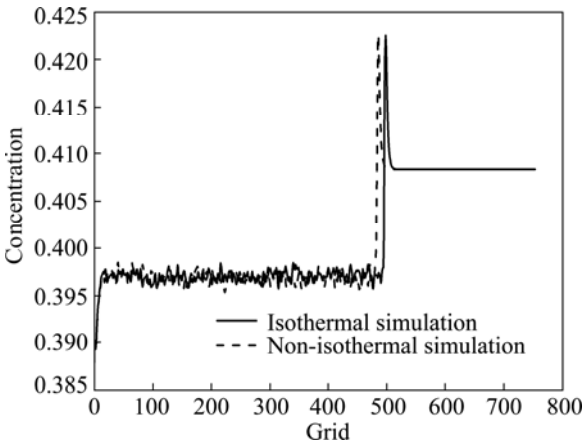

Fig. 4 Concentration profiles in growth direction through dendritic tip

In order to investigate the tip operating behavior under non-isothermal condition, the effect of the interfacial width on the growth speed is shown in Fig. 5. It can be found that, the dendrite growth is obviously restrained by the interfacial width. With increase of the interfacial width, the fluctuation wavelength of the dendritic tip velocity declines apparently, and the fluctuation cycle increases markedly. When the interfacial width δ=7.2×10^{-6} cm, the tip velocity is convergent to a stable value, about 1.3 cm/s. But, it should be noted that the real interfacial width of metal is about 10^{-8} cm, so the acute fluctuation of the tip velocity is consistent with the actual solidification.

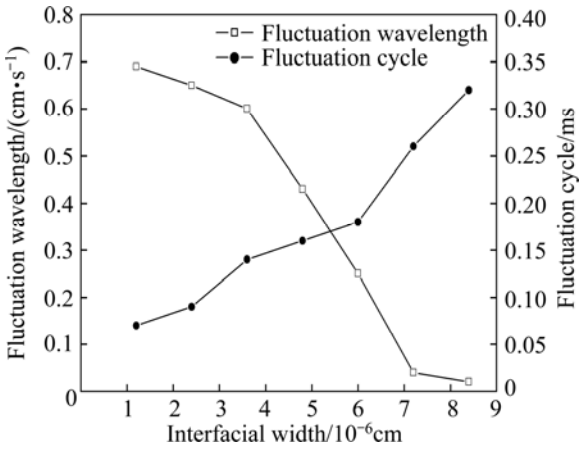

Fig. 5 Effect of interfacial width on tip operating behavior

In order to investigate the consistency between the isothermal PFM and the non-isothermal PFM, the effect of the thermal diffusivity D_T on the interfacial profile is investigated, as shown in Fig. 6. It can be found that, the thermal diffusion layer is thick at large D_T, and the heat generated by solidification can be quickly spread out, so the temperature rises more slowly in the solidifying zone. With decrement of D_T, the thermal diffusion layer becomes thin, and the latent heat release is resorted in the solidifying zone, thus the simulation results are gradually consistent with the isothermal simulation. Due to the fact that release of the latent heat is little at a small D_T, the effect of the latent heat on the thermal distribution in the original melt is trivial, then the undercooling degree of the melt is high. So, the growth of the dendrite is successive, and the morphology is ripened and developed, which is consistent with the result of isothermal simulation.

5 Conclusions

1) A non-isothermal phase field model of binary alloy is progressed for simulating the interfacial

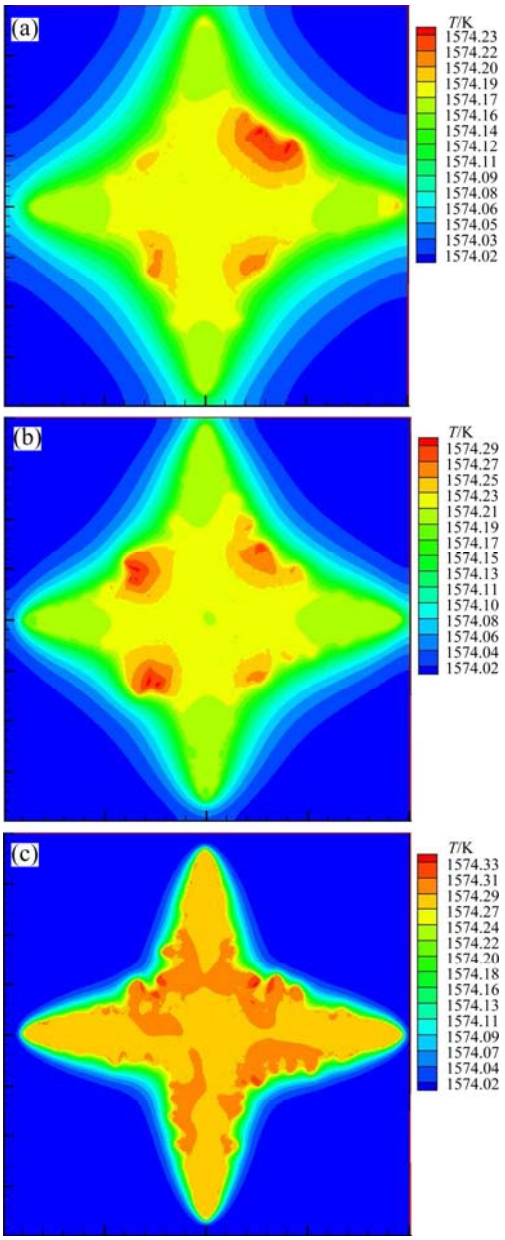

Fig. 6 Temperature field profile under different D_T: (a) D_T=0.155 cm^2/s; (b) D_T=0.08 cm^2/s; (c) D_T=0.02 cm^2/s

morphology profiles. The explicit difference method is implemented to solve the phase field and solute field controlled equations, and the alternating direction implicit(ADI) algorithm is employed to solve the thermal diffusion equation.

2) The non-isothermal simulation results are closer to the actual solidification process of binary alloys compared with the isothermal simulation results. In the non-isothermal solidification process, the temperature increases in the solidifying zone, and recalescence occurs. Then, dendrite grows corresponding with thick thermal diffusion layers. The solute diffuses more sufficiently in the condition of non-isothermal solidification. The tip velocity of non-isothermal simulation fluctuates acutely comparative to isothermal solidification, and the fluctuation cycle is about 0.1 ms. With increase of the interfacial width, the fluctuation wavelength of the dendritic tip velocity declines apparently, and the fluctuation cycle increases markedly. Because the solute diffusivity is so small, the micro-segregation is severe in both solidifying conditions. When the thermal diffusivity decreases, the non-isothermal PFM is gradually consistent with the isothermal PFM.

Appendix

ADI algorithm for solving thermal diffusion Equation (3)

In the first time step Δt, the explicit difference method is employed to solve the equation in x-axis direction, and the implicit difference method is employed to solve the equation in y-axis direction. It can be written as

$$\frac{{T_{i,j}}^{n+1}-{T_{i,j}}^{n}}{\Delta t}+\left[(1-c)L^{\mathrm{A}}+cL^{\mathrm{B}}\right]\cdot\frac{p'(\phi)}{c_p}\cdot\frac{\partial\phi}{\partial t}=D_T\frac{{T_{i+1,j}}^{n+1}-2{T_{i,j}}^{n+1}+{T_{i-1,j}}^{n+1}}{\Delta x^2}+D_T\frac{{T_{i,j+1}}^{n}-2{T_{i,j}}^{n}+{T_{i,j-1}}^{n}}{\Delta y^2}$$

where n is time node, and the term of $\Delta t\Delta x^2$ is multiplied to both sides of the equation,

$$\Delta x^2{T_{i,j}}^{n+1}-\Delta x^2{T_{i,j}}^{n}+\Delta t\Delta x^2\left[(1-c)L^{\mathrm{A}}+cL^{\mathrm{B}}\right]\cdot\frac{p'(\phi)}{c_p}\cdot\frac{\partial\phi}{\partial t}=\Delta tD_T\left({T_{i+1,j}}^{n+1}-2{T_{i,j}}^{n+1}+{T_{i-1,j}}^{n+1}\right)+\Delta tD_T\left({T_{i,j+1}}^{n}-2{T_{i,j}}^{n}+{T_{i,j-1}}^{n}\right)$$

Then both sides of the equation are divided by ΔtD_T,

$$-{T_{i-1,j}}^{n+1}+\left(\frac{\Delta x^2}{\Delta tD_T}+2\right){T_{i,j}}^{n+1}-{T_{i+1,j}}^{n+1}+\frac{\Delta x^2}{D_T}\left[(1-c)L^{\mathrm{A}}+cL^{\mathrm{B}}\right]\cdot\frac{p'(\phi)}{c_p}\cdot\frac{\partial\phi}{\partial t}={T_{i,j+1}}^{n}+\left(\frac{\Delta x^2}{\Delta tD_T}-2\right){T_{i,j}}^{n}+{T_{i,j-1}}^{n}$$

The above equation is solved by setting the following formations:

$$a_i=1,\ \ i\in[2,N];\ \ b_i=\frac{\Delta x^2}{\Delta tD_T}+2,\ \ i\in[1,N];$$

$$c_i=1,\ \ i\in[1,N-1];$$

$$d_i={T_{i,j+1}}^{n}+\left(\frac{\Delta x^2}{\Delta tD_T}-2\right){T_{i,j}}^{n}+{T_{i,j-1}}^{n}-$$

$$\frac{\Delta x^2}{D_T}\left[(1-c)L^{\mathrm{A}}+cL^{\mathrm{B}}\right]\cdot\frac{p'(\phi)}{c_p}\cdot\frac{\partial\phi}{\partial t},\quad i\in[1,N]$$

where N is the whole number, and $N>0$, So, the thermal diffusion equation can be dispersed as

$$-a_i{T_{i-1,j}}^{n+1}+b_i{T_{i,j}}^{n+1}-c_i{T_{i+1,j}}^{n+1}=d_i$$

In the second time step Δt, the implicit difference method is employed to solve the equation in x-axis direction, and the explicit difference method is employed to solve the equation in y-axis direction. So, the thermal diffusion equation can be dispersed as

$$-a_i{T_{i,j-1}}^{n+1}+b_i{T_{i,j}}^{n+1}-c_i{T_{i,j+1}}^{n+1}=d_i$$

where

$$a_i=1,\quad i\in[2,N];\quad b_i=\frac{\Delta x^2}{\Delta t D_T}+2,\quad i\in[1,N];$$

$$c_i=1,\quad i\in[1,N-1];$$

$$d_i={T_{i+1,j}}^{n}+\left(\frac{\Delta x^2}{\Delta t D_T}-2\right){T_{i,j}}^{n}+{T_{i-1,j}}^{n}-\frac{\Delta x^2}{D_T}\left[(1-c)L^{\mathrm{A}}+cL^{\mathrm{B}}\right]\cdot\frac{p'(\phi)}{c_p}\cdot\frac{\partial\phi}{\partial t},\quad i\in[1,N].$$

References

[1] MAXWELL I, HELLAWELL A. A simple model for grain refinement during solidification [J]. Acta Metall, 1975, 23: 229−237.

[2] WOLFRAM S. Cellular automata as models of complexity [J]. Nature, 1984: 311: 419−448.

[3] SAITO Y, GOLDBECK-WOOD G, MULLER-KRUMBHAAR H. Numerical simulation of dendritic growth [J]. Phys Rev A, 1988, 38(4): 2148−2153.

[4] SPITTLE J A, BROWN S G R. Computer simulation of the effects of alloy variables on the grain structures of castings [J]. Acta Metall, 1989, 37(7): 1803−1810.

[5] FIFE P C, GILL S G. The phase-field description of mushy zones [J]. Phys D, 1989, 35: 267−275.

[6] KOBAYASHI R. Modeling and numerical simulation of dendritic crystal growth [J]. Phys D, 1993, 63: 410−423.

[7] WANG Gang, ZENG De-chang, LIU Zhong-wu. Phase field calculation of interface mobility in a ternary alloy [J]. Transactions of Nonferrous Metals Society of China, 2012, 22(7): 1711−1716.

[8] ZHANG Shu-zhou, ZHANG Rui-jie, QU Xuan-hui, FANG Wei, LIU Ming-zhi. Phase field simulation for non-isothermal solidification of multicomponent alloys coupled with thermodynamics database [J]. Transactions of Nonferrous Metals Society of China, 2013, 23(8): 2361−2367.

[9] WHEELER A A, BOETTINGER W J, MCFADDEN G B. Phase-field model for isothermal phase transition in binary alloy [J]. Phys Rev E, 1992, 45(10): 7424−7439.

[10] WANG Zhi-ping, WANG Jun-wei, ZHU Chang-sheng, FENG Li, XIAO Rong-zhen. Phase-field simulations of forced flow effect on dendritic growth perpendicular to flow [J]. Transactions of Nonferrous Metals Society of China, 2011, 21(3): 612−617.

[11] WANG Jun-wei, ZHU Chang-sheng, WANG Zhi-ping, FENG Li, XIAO Rong-zhen. Phase-field simulation of forced flow effect on random preferred growth direction of multiple grains [J]. Transactions of Nonferrous Metals Society of China, 2011, 21(7): 1620−1626.

[12] WHEELER A A, BOETTINGER W J, MCFADDEN G B. Phase field model of trapping during solidification [J]. Phys Rev E, 1993, 47(4): 1893−1909.

[13] CONTI M. Solute trapping in directional solidification at high speed: A one-dimensional study with the phase-field model [J]. Phys Rev E, 1997, 56: 3717−3720.

[14] AHMAD N A, WHEELER A A, BOETTINGER W J, MCFADDEN G B. Solute trapping and solute drag in a phase-field model of rapid solidification [J]. Phys Rev E, 1998, 58(3): 3436−3450.

[15] KIM S G, KIM W T, SUZUKI T. Interfacial compositions of solid and liquid in a phase-field model with finite interface thickness for isothermal solidification in binary alloys [J]. Phys Rev E, 1998, 58(3): 3316−3323.

[16] KIM S G, KIM W T, SUZUKI T. Phase-field model for binary alloys [J]. Phys Rev E, 1999, 60(6): 7186−7197.

[17] CONTI M. Solidification of binary alloys: Thermal effects studied with the phase-field model [J]. Phys Rev E, 1997, 55(1): 765−771.

[18] LOGINOVA I, AMBERG G, AGERN J. Phase-field simulation of non-isothermal binary alloy solidification [J]. Acta Mater, 2001, 49: 573−581.

[19] OHNO M. Quantitative phase-field modeling of nonisothermal solidification in dilute multicomponent alloys with arbitrary diffusivities [J]. Phys Rev E, 2012, 86: 051603-1.

[20] WARREN J A, BOETTINGER W J. Prediction of dendritic growth and microsegregation patterns in a binary alloy using the phase-field method [J]. Acta Metal Mater, 1995, 43(2): 689−703.

[21] XIAO Rong-zheng, WANG Zhi-ping, ZHU Chang-sheng, LI Wen-sheng, FENG Li. Influence of anisotropy on dendritic growth in binary alloy with phase-field simulation [J]. ISIJ INT, 2009, 49(8): 1156−1160.

相场法对比模拟二元合金等温/非等温凝固过程

肖荣振，安国升，朱昶胜，王智平，杨世银

兰州理工大学 甘肃省有色金属新材料省部共建国家重点实验室，兰州 730050

摘　要：基于熵函数建立二元合金的二维相场模型，采用基于均匀网格的有限差分法求解相场和溶质场控制方程；为了避免时间步长的限定，采用交替隐式差分法(ADI)求解温度场控制方程。对 Ni−Cu 合金非等温凝固过程的部分特征进行模拟研究，对比分析二元合金等温/非等温凝固过程。模拟结果表明：非等温模型更能有效地模拟二元合金的实际凝固过程，并且随着热扩散系数的减小，非等温相场模型逐渐向等温相场模型回归。

关键词：相场法；二元合金；等温凝固；非等温凝固

(Edited by Xiang-qun LI)